

OPEN ACCESS

EDITED BY

Francesco Cuccia, ARNAS Ospedali Civico Di Cristina Benfratelli, Italy

REVIEWED BY
Qianqian Li,
Institute of Basic Medical Sciences, China
Ningbo Liu,
Tianjin Medical University, China

*CORRESPONDENCE

Fuli Zhang

Jianfeng Qiu

Yinglun Sun

[†]These authors have contributed equally to this work

RECEIVED 19 July 2025 ACCEPTED 03 November 2025 PUBLISHED 20 November 2025

CITATION

Liu Y, Pan Y, Wang Q, Jiang H, Lu N, Chen D, Yu Y, Gao Y, Zhang H, Sun Y, Qiu J and Zhang F (2025) Integration of intratumoral/ peritumoral radiomics and deep learning for predicting overall survival in non-small cell lung cancer patients: a multicenter study. *Front. Oncol.* 15:1669200. doi: 10.3389/fonc.2025.1669200

COPYRIGHT

© 2025 Liu, Pan, Wang, Jiang, Lu, Chen, Yu, Gao, Zhang, Sun, Qiu and Zhang. This is an open-access article distributed under the terms of the Creative Commons Attribution License (CC BY). The use, distribution or reproduction in other forums is permitted, provided the original author(s) and the copyright owner(s) are credited and that the original publication in this journal is cited, in accordance with accepted academic practice. No use, distribution or reproduction is permitted which does not comply with these terms.

Integration of intratumoral/ peritumoral radiomics and deep learning for predicting overall survival in non-small cell lung cancer patients: a multicenter study

Yongxin Liu^{1,2†}, Yuteng Pan^{2†}, Qiusheng Wang³, Huayong Jiang¹, Na Lu¹, Diandian Chen¹, Yanjun Yu¹, Yanxiang Gao¹, Huijuan Zhang¹, Yinglun Sun^{2*}, Jianfeng Qiu^{4*} and Fuli Zhang^{1*}

¹Radiation Oncology Department, The Seventh Medical Center of Chinese People's Liberation Army PLA General Hospital, Beijing, China, ²School of Radiology, Shandong First Medical University and Shandong Academy of Medical Sciences, Taian, China, ³School of Automation Science and Electrical Engineering, Beihang University, Beijing, China, ⁴The First Affiliated Hospital of Shandong First Medical University, Jinan, China

Background: Prognostic assessment of non-small cell lung cancer (NSCLC) relies on TNM staging, yet tumor heterogeneity limits its accuracy. This study aimed to develop a model for improving the prediction of overall survival (OS) in NSCLC patients receiving radiotherapy, which integrated intratumoral/peritumoral radiomics features and 3D deep learning (DL) features.

Methods: A total of 303 NSCLC patients from three centers were retrospectively enrolled. Radiomics features were extracted from intratumoral and 3/6/9 mm peritumoral regions on CT scans. A network named 3D-SE-ResNet was proposed to extract DL features. Lasso-Cox and principal component analysis (PCA) were used to integrate multidimensional features to establish a combined model. Performance was evaluated via the concordance index (C-index) and area under the curve (AUC). Survival differences were visualized through Kaplan–Meier curves.

Results: The 6 mm expansion peritumoral radiomics features analysis showed the best performance (C-index: 0.63). The DL features outperformed the radiomics features (C-index: 0.74 vs 0.63). The combined model achieved the highest accuracy (C-index: 0.77/0.73 across datasets). K–M analysis confirmed significant survival differences (log-rank P < 0.001).

Conclusion: The combined model integrates intratumoral/peritumoral radiomics features and 3D DL features and effectively predicts the OS of NSCLC patients, offering a novel tool for personalized radiotherapy strategies.

KEYWORDS

non-small cell lung cancer, CT, radiomics, deep learning, overall survival

Introduction

Non-small cell lung cancer (NSCLC) is a leading cause of cancer-related mortality worldwide, accounting for 80%–85% of all lung cancer cases (1–3). Radiotherapy (RT) plays a pivotal role in the therapeutic management of NSCLC patients. However, the current 5-year survival rate remains below 30% (4–6), highlighting the urgent need for precise prognostic stratification to optimize RT strategies and adjuvant therapeutic decisions.

The conventional TNM staging system has limited predictive accuracy because of its inability to capture the heterogeneity of the tumor microenvironment (7, 8). Radiological assessment is limited in quantifying tumor information because of its heavy reliance on subjective experience. Radiomics has shown substantial potential in tumor prognosis prediction (9–11). Accumulated evidence indicates that the peritumoral lung parenchyma, a key pathway for tumor dissemination, is closely linked to recurrence and poor prognosis (12–14). Peritumoral radiomics, which quantifies heterogeneity in surrounding regions, has been shown to effectively capture microenvironmental dynamics and enhance prognostic predictions (15–17). Nevertheless, the optimal expansion distance of peritumoral regions of interest (ROIs) remains controversial across studies, which may hinder their clinical generalizability (18–20).

The integration of artificial intelligence (AI) with radiomics offers a novel direction for prognostic modeling. Compared with conventional 2D convolutional neural networks (CNNs), 3D CNNs can more comprehensively capture three-dimensional spatial heterogeneity and have demonstrated superiority in tasks such as pulmonary nodule classification (21-23). However, limitations exist, including overfitting risks due to limited medical imaging datasets and a shortage of networks optimized for survival analysis. We propose a novel network architecture named 3D-SE-ResNet, which embeds a squeeze-and-excitation (SE) module into the 3D ResNet framework to achieve adaptive feature channel calibration. Furthermore, this study establishes a novel paradigm for personalized prognosis by synergistically integrating intratumoral/ peritumoral radiomics features with 3D deep learning (DL) features through a principal component analysis (PCA)-driven fusion strategy.

This study aimed to construct a multicenter-validated combined model for predicting overall survival (OS) in NSCLC patients undergoing RT by integrating intratumoral/peritumoral radiomics features and 3D DL features. These advancements aim to

Abbreviations: AUC, area under the curve; CI, confidence interval; C-index, concordance index; CNNs, convolutional neural networks; CT, computed tomography; CTV, clinical target volume; DL, deep learning; GAP, global average pooling; GTV, gross tumor volume; HR, hazard ratio; Lasso, least absolute shrinkage and selection operator; LoG, Laplacian of Gaussian; NSCLC, non-small cell lung cancer; OS, overall survival; PCA, principal component analysis; ROI, region of interest; RT, radiotherapy; SE, squeeze-and-excitation.

provide a robust tool for optimizing individualized radiotherapy strategies.

Materials and methods

Patients data

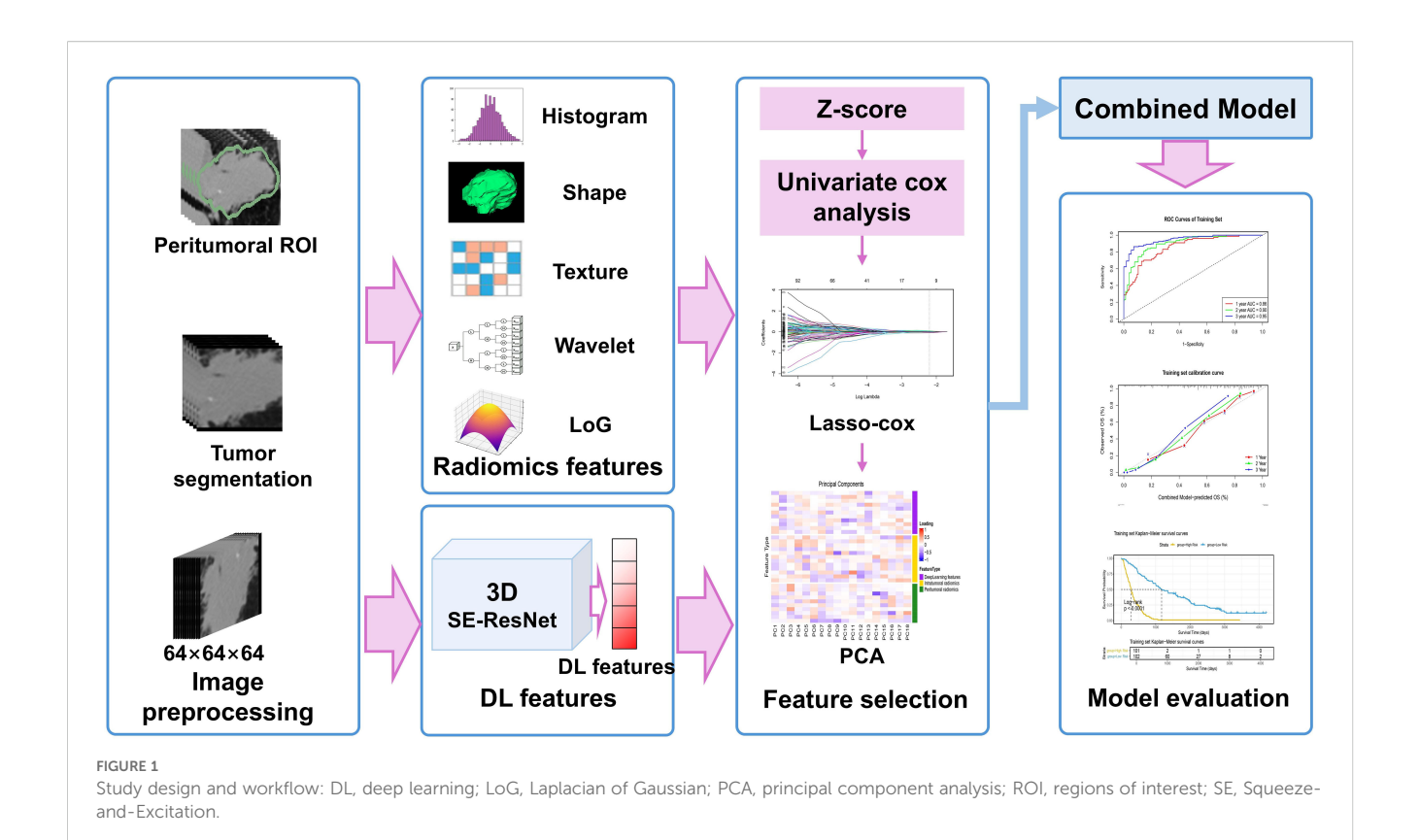
This multicenter retrospective study included 303 non-small cell lung cancer (NSCLC) patients from three centers. The training set included 203 adenocarcinoma and squamous cell carcinoma patients from the publicly available MAASTRO Clinic dataset (24), with the study dates (from the metadata file) ranging from November 2004 to January 2014. The test set included 100 histologically confirmed adenocarcinoma or squamous cell carcinoma patients enrolled between January 2016 and August 2021 (68 from the Seventh Medical Center of Chinese PLA General Hospital and 32 from Shandong Provincial Hospital Affiliated with Shandong First Medical University), all of whom met the following criteria.

The inclusion criteria were as follows: (1) histologically verified NSCLC (adenocarcinoma or squamous cell carcinoma); (2) aged >18 years; (3) received radiotherapy or chemoradiotherapy; (4) available radiotherapy planning CT scans; and (5) complete clinical records. The exclusion criteria included the following: (1) the presence of other primary malignancies; (2) poorly defined tumor boundaries; and (3) loss to follow-up.

The protocol was conducted in compliance with the Declaration of Helsinki and has been approved by the Ethics Committee of the Seventh Medical Center of Chinese PLA General Hospital (No. S2025-030-01) and the Ethics Committee of Shandong First Medical University (No. SB-KJCX2101). Owing to the retrospective nature of the study and the use of anonymized data, written informed consent was waived. The study workflow is shown in Figure 1.

Treatment and follow-up

In the training set, patients with stage N2/N3 and T4 disease were required to first receive 3 cycles of induction chemotherapy with gemcitabine combined with cisplatin or carboplatin, and radiotherapy was initiated at least 14 days after the completion of chemotherapy. All radiotherapy was performed in accordance with the principles that mean lung dose (MLD) \leq 19 Gy and the maximum spinal cord dose \leq 54 Gy, with a maximum radiation dose of 79.2 Gy. Among these patients, a fractionation schedule of 1.8 Gy per fraction (twice daily) was adopted for those undergoing radical radiotherapy with a minimum of 8 h between the two fractions. Three dimensional conformal radiotherapy (3D-CRT) or intensity modulated radiotherapy (IMRT) techniques were used. For patients undergoing concurrent chemoradiotherapy, 2 cycles of chemotherapy were completed first, followed by irradiation of 45 Gy at 1.5 Gy per fraction (twice daily); thereafter, the fractionation



schedule was adjusted to 2.0 Gy per fraction (once daily) for a boost irradiation of 6-24 Gy.

All patients in the test set underwent definitive radiotherapy (RT) or chemoradiotherapy. The RT target volume covered the primary lesion and involved lymph nodes, with a conventional fractionation schedule: 2 Gy per fraction, five fractions per week, and a total dose of 50-60 Gy. RT techniques were implemented according to the clinical routines of the participating centers: the Seventh Medical Center of Chinese PLA General Hospital adopted intensity-modulated radiotherapy (IMRT) or volumetric modulated arc therapy (VMAT), while Shandong Provincial Hospital used IMRT. For VMAT, two full arcs were used; for IMRT, 5-7 coplanar fields were used. For patients undergoing chemoradiotherapy, platinum-based dual-drug combination regimens were mainly adopted: etoposide combined with cisplatin (EP regimen) was preferred for patients with squamous cell carcinoma; pemetrexed combined with cisplatin or carboplatin (PC regimen) was recommended for patients with non-squamous cell carcinoma; in addition, paclitaxel combined with carboplatin was also an alternative regimen for cisplatin-intolerant patients.

The baseline clinical characteristics included sex, age, histologic subtype, TNM stage, and overall stage. The study's major outcome measure was OS, which was calculated from the commencement of RT to either mortality occurrence or censoring at the final follow-up (August 2024). Patients in the test set were followed every 3 months during the initial postdiagnosis year and every 6–12 months thereafter, with a minimum follow-up of 36 months. Survival outcomes for the training set were derived from the publicly available dataset (24).

Image acquisition and preprocessing

RT planning CT scans were performed on Philips and Siemens large-bore simulation scanners, covering the thoracic region with a tube voltage of 120 kV, slice thickness of 2–5 mm, and a reconstruction matrix of 512×512 . To mitigate variability from multicenter imaging protocols, CT images were preprocessed as follows: DICOM files were converted to NIFTI format, followed by isotropic resampling with B-spline interpolation to standardize the voxel dimensions to $1\times1\times1$ mm³.

ROI segmentation and radiomics feature extraction

The intratumoral region of interest (ROI) was defined as the gross tumor volume (GTV) by an experienced radiation oncologist (working for over 20 years). To evaluate the prognostic impact of peritumoral regions, three concentric peritumoral expansions (3/6/9 mm) were generated via SimpleITK (v 2.3.1). Radiomics features were extracted using PyRadiomics (v 3.1) with the following parameters: intensity normalization enabled and a bin width of 25 for histogram discretization. A total of 1316 radiomics features were extracted from each ROI, encompassing five categories: first-order statistics (n=18), shape-based features (n=14), texture features (n=75), wavelet-filtered features (n=744), and Laplacian of Gaussian (LoG)-filtered features (n=465, with sigma values set to [1.0, 2.0, 3.0, 4.0, 5.0]).

Deep learning network establishment

The 3D-SE-ResNet architecture was systematically adapted from ResNet18 to accommodate 3D survival analysis tasks. As illustrated in Figure 2, the network comprises three core components: (1) a backbone module containing an initial 3D convolutional layer (kernel size=3×3×3, stride=2) for spatial downsampling and preliminary feature extraction, which is followed by a 3D max-pooling layer (kernel size = 3×3×3, stride = 2) to further reduce spatial dimensions. (2) Four sequential residual blocks with a progressively increasing number of filters (64, 128, 256, 512). Each residual block contains two 3D convolutional basic units, both utilizing 3×3×3 kernels combined with batch normalization and ReLU activation, and employs skip connections to mitigate the gradient vanishing problem. The first unit's convolutional layer in the first residual block acts directly on the input, while the second unit's convolutional layer follows a "BN +ReLU+convolution" architecture; both units use a convolution stride of 1. In subsequent residual blocks, the first unit's convolution uses a stride of 2, and the second unit uses a stride of 1, with both units adopting the "BN+ReLU+convolution" architecture for their convolutional layers. (3) A squeeze-and-excitation (SE) module integrated after each residual block to implement the channel attention mechanisms.

The SE module performs feature recalibration through three steps (with a compression ratio of 64): (1) Spatial compression: Generating channel-wise statistics via global average pooling (GAP), transforming each 3D feature map (H×W×D×C, where C is the number of channels) into a 1D vector (1×1×1×C). (2) Channel dependency modeling: Establishing inter-channel dependencies through two fully connected layers. The first fully connected layer reduces the dimension to C/64 with ReLU activation, and the second restores the dimension to C with sigmoid activation, generating channel weights (range: 0–1). (3) Feature map rescaling: Adaptive enhancement of prognosis-relevant channels and suppression of irrelevant signals via element-wise multiplication between the original feature maps and the learned channel weights. The network terminates with

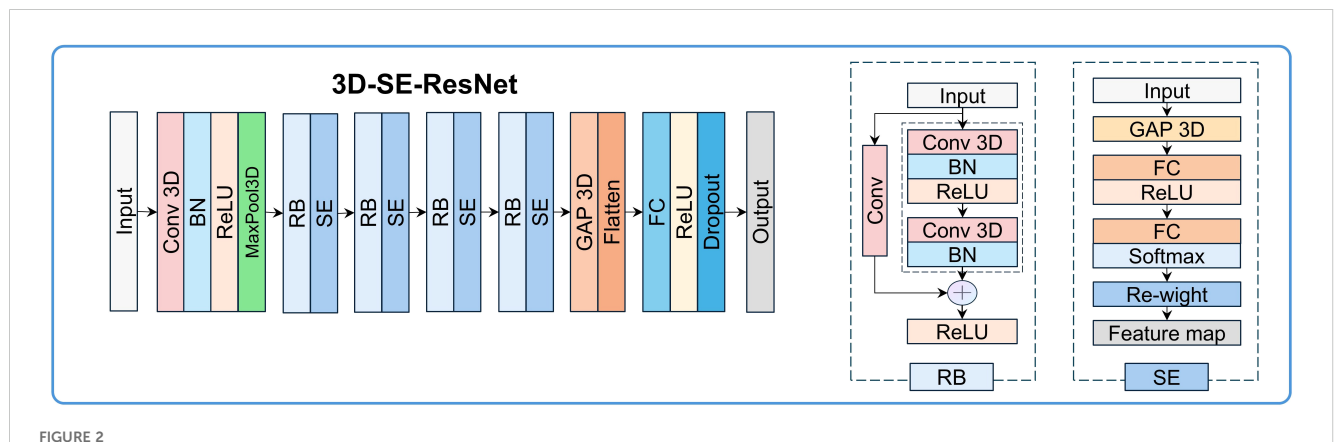
fully connected layers (512 \rightarrow 512 \rightarrow 256 \rightarrow 128 units), dropout (rate=0.4), and L2 regularization (λ =1e-4). The output layer uses tanh activation for survival prediction. Ablation experiments were conducted to validate the contribution of the SE module.

Deep learning network training and feature extraction

The model training encompassed three phases: preprocessing, augmentation, and optimization. Intratumoral ROIs were resized to 64×64×64 via linear interpolation and normalized via Z score transformation. To increase data diversity, seven types of 3D augmentations were implemented, including contrast adjustment, brightness scaling, gamma correction, Gaussian noise addition, blurring, 3D mirroring, and spatial rotation, with the technical specifications provided in Table 1. Network optimization employs the Cox negative partial likelihood loss function (25), which is optimized via the Adam optimizer with an initial learning rate of 1×10^{-4} , exponentially decayed by a factor of 0.96 every 1000 steps, and a batch size of 32. Training proceeded for 100 epochs with early stopping triggered if the validation loss plateaued for 15 consecutive epochs. The feature vectors (512-dimensional) were extracted from the GAP layer post training. All the implementations utilized TensorFlow 2.7 on an NVIDIA GeForce RTX 4070 Ti GPU with CUDA 11.2 acceleration.

Feature selection and model development

The feature selection procedures were restricted to the training set. For radiomics and deep learning features, a three-step process was applied: (1) Z score normalization to standardize feature scales; (2) univariate cox analysis (P < 0.05) to identify survival-associated features; and (3) least absolute shrinkage and selection operator (Lasso) Cox regression with standard 10-fold cross-validation to retain nonzero coefficients. The feature selection workflow is illustrated in Figure 1. A radiomics/deep learning signature was



3D-SE-ResNet framework diagram: BN, batch normalization; Conv, convolution layer; FC, fully connected layer; GAP, global average pooling layer; RB, residual block.

TABLE 1 Technical details of 3D data augmentation.

Augmentation type	Parameter settings	Probability
Contrast Adjustment	Multiplier range (1.0-1.75)	15%
Brightness Multiplicative Adjustment	Scaling factor (0.7-1.5)	15%
Gamma Correction	γ range (0.5-2.0)	15%
Gaussian Noise	Variance range (0-0.05)	15%
Gaussian Blur	σ range (0.5-1.5)	15%
3D Mirroring	Random flipping along X/Y/ Z axes	30%
3D Spatial Rotation	Rotation (0-360°) around Z-axis	30%

derived via a linear combination of selected features and their coefficients.

Principal component analysis (PCA) was performed on the integrated intratumoral/peritumoral radiomics and deep learning features, retaining components accounting for \geq 95% of the cumulative variance. Factor loading heatmaps were used to visualize the contribution of each feature to the principal components. Within the training set, the dimensionality-reduced features were integrated to construct the combined predictive model.

Model validation and evaluation

Model discrimination was assessed via Harrell's concordance index (C-index) and area under the curve (AUC) from receiver operating characteristic curve (ROC) analysis. Calibration curves (bootstrap resampling: 1000 iterations) were used to evaluate the agreement between the predicted and observed survival probabilities. Patients were stratified into low/high-risk subgroups through the median risk score in the training set to determine the optimal cutoff value.

To further evaluate the model's utility in personalized risk stratification, subgroup analyses were conducted. Specifically, we stratified patients by overall stage (Stage I - II vs. Stage III), histologic subtype (adenocarcinoma vs. squamous cell carcinoma), gender (male vs. female), and age (≥ 65 years vs. < 65 years) in both the training and test sets. For each subgroup, survival differences between cohorts were analyzed via the Kaplan–Meier method with log - rank tests, and the corresponding Kaplan–Meier curves were plotted.

Statistical analysis

Statistical computations were conducted with R v4.4.0 and Python 3.9. Categorical variables were evaluated via Fisher's exact test or the chi-square test; for continuous variables, normality was first determined using the Shapiro-Wilk test, with the independent t

test applied for normally distributed variables and the Mann-Whitney U test for non-normally distributed variables. DeLong's test was used to compare differences in AUC values between the single signature and combined models. Subgroup analyses stratified by clinical characteristics (tumor stage, histological type, age, and gender) were performed in both the training and testing sets; for survival-related outcomes, the log-rank test was employed to compare survival differences between subgroups. All hypothesis tests were two-tailed with a significance threshold set at α =0.05.

Results

Patient cohort characteristics

A total of 303 non-small cell lung cancer (NSCLC) patients from three centers were included in this study. The baseline clinical characteristics of all patients are listed in Table 2.

Radiomics feature analysis

From the intratumoral and peritumoral regions (3 mm, 6 mm, and 9 mm expansions), 1316 radiomics features were extracted. Univariate cox regression identified 214 significant intratumoral radiomics features and 83, 88, and 125 peritumoral radiomics features, respectively. Subsequent Lasso-Cox analysis further refined these features to 12 intratumoral and 9, 10, and 10 peritumoral key radiomics features. To explore the synergistic effects of the intratumoral and peritumoral regions, combined radiomics signatures were generated by integrating selected radiomics features from both regions. Predictive performance varied significantly across peritumoral expansion distances and their combinations (Table 3). Among the standalone peritumoral radiomics signatures, the 6-mm expansion radiomics signature achieved the highest C-index (0.63, 95% CI: 0.58-0.67), whereas the combined Rad+Rad_6 mm radiomics signature further improved the C-index (0.65, 95% CI: 0.60-0.69); thus, this radiomics signature was selected as the standardized peritumoral region. The names and corresponding coefficients of all features within the Rad + Rad_6 mm radiomics signature are presented in Figure 3.

Deep learning feature analysis

Among 512 deep learning (DL) features extracted from 3D-SE-ResNet, 11 key prognostic features were retained after univariate cox and Lasso-Cox screening. Compared with the intratumoral and 6-mm peritumoral radiomics signatures, the DL signature showed a trend of improved discriminative performance, with a C-index of 0.74 (95% CI: 0.70-0.77) in the training set and 0.66 (95% CI: 0.58–0.73) in the test set. Ablation experiments confirmed the critical role of the SE module: its integration yielded a 13.8% performance gain in the 3D-ResNet model (C-index: 0.74 vs. 0.65), indicating that the

TABLE 2 Clinical characteristics of all patients.

Characteristics	Training set (n=203)	Test set (n=100)	P value
Age	69 (63–77)	66 (57–72)	0.01
Sex			0.09
Male	144(70.9%)	80(80.0%)	
Female	59(29.1%)	20(20.0%)	
Histology			0.03
Adenocarcinoma	51(25.1%)	42(42.0%)	
Squamous	152(74.9%)	58(58.0%)	
T Stage			0.30
1	37(18.2%)	20(20.0%)	
2	77(37.9%)	32(32.0%)	
3	32(15.8%)	24(24.0%)	
4	57(28.1%)	24(24.0%)	
N Stage			0.12
0	81(39.9%)	26(26.0%)	
1	16(7.9%)	10(10.0%)	
2	65(32.0%)	37(37.0%)	
3	39(19.2%)	27(27.0%)	
4	2(1.0%)	0(0%)	
M Stage			0.10
0	202(99.5%)	98(98.0%)	
1	0(0.0%)	2(2.0%)	
3	1(0.5%)	0(0%)	
Overall Stage			0.22
I	34(16.7%)	14(14.0%)	
II	31(15.3%)	13(13.0%)	
IIIA	58(28.6%)	28(28.0%)	
IIIB	80(39.4%)	45(45.0%)	
Survival Time (days)	493 (252–1217)	786 (509–1024)	0.03

SE module effectively enhances the extraction of prognosis-related features. As shown in Figure 4, the AUC values of the 3D-SE-ResNet DL signature for predicting 1-, 2-, and 3-year overall survival were higher than those of the baseline model at all timepoints.

Combined model development and validation

Principal component analysis (PCA) was applied to integrate intratumoral radiomics, 6-mm peritumoral radiomics, and DL

features, with the distribution of feature contributions across principal components visualized in Figure 5. The combined model, which integrates PCA-reduced features, achieved C-index values of 0.77 (95% CI: 0.75–0.81) in the training set and 0.73 (0.72–0.86) in the test set, outperforming individual signatures. ROC analysis revealed AUCs of 0.86 (95% CI: 0.81–0.90), 0.90 (0.86–0.94), and 0.95 (0.92–0.97) for predicting 1-, 2-, and 3-year OS, respectively (Table 4), with the corresponding ROC curves illustrated in Figure 6.

Risk stratification and survival analysis

Calibration analyses revealed high concordance between the predicted and observed survival probabilities (Figure 7). Patients were stratified into high-risk and low-risk groups by applying a risk threshold (cutoff value = 1.14), which was derived from the combined model's median risk score. The high-risk group had a significantly poorer prognosis compared to the low-risk group in both datasets: the hazard ratio (HR) for the training set was 5.39 (95% CI: 3.83–7.59), and for the test set was 4.48 (95% CI: 2.54–7.91). Kaplan–Meier analysis further confirmed significant survival differences between the two risk groups (log-rank P < 0.0001 for both datasets; Figure 8).

To comprehensively evaluate the personalized risk stratification ability of the combined model, subgroup analyses were performed within clinically relevant strata. The model demonstrated consistent risk discrimination capabilities across gender subgroups (Figure 9), age subgroups (Figure 10), histologic subtype subgroups (Figure 11), and overall stage subgroups (Figure 12). Statistically significant survival differences were observed between high - and low - risk groups in both the training and test sets (log - rank test, P < 0.05), validating its robustness across patient populations with diverse clinical characteristics.

Discussion

This study developed a multicenter-validated combined model that integrates intratumoral/peritumoral radiomics features and 3D deep learning features to predict overall survival (OS) in non-small cell lung cancer (NSCLC) patients undergoing radiotherapy. The results demonstrated that radiomics features from the 6-mm peritumoral region exhibited optimal prognostic value (C-index=0.63), whereas deep learning (DL) features extracted by 3D-SE-ResNet significantly outperformed conventional radiomics features (C-index=0.74 vs. 0.63). The combined model achieved a C-index of 0.73 in the test set and an AUC of 0.86 for 3-year OS prediction, outperforming the conventional TNM staging system (AUC \approx 0.65) (26, 27) and validating the efficacy of the multidimensional feature fusion strategy. These findings provide a novel framework for individualized prognostic assessment in NSCLC radiotherapy.

The aggressive nature of NSCLC leads to destruction of adjacent lung structures, leading to the infiltration of vasculo-lymphatic

TABLE 3 Comparison of C-index (95%CI) for intratumoral/peritumoral radiomics signatures with different expansion distances.

Signatures	Training set	Test set
Rad	0.63 (0.58-0.68)	0.61 (0.48-0.68)
Rad_3mm	0.61 (0.57-0.65)	0.61 (0.49-0.68)
Rad_6mm	0.63 (0.58-0.67)	0.62 (0.49-0.69)
Rad_9mm	0.61 (0.57-0.65)	0.59 (0.46-0.66)
Rad+Rad_3mm	0.64 (0.60-0.69)	0.63 (0.52-0.70)
Rad+Rad_6mm	0.65 (0.60-0.69)	0.64 (0.53-0.70)
Rad+Rad_9mm	0.64 (0.59-0.69)	0.62 (0.51-0.71)

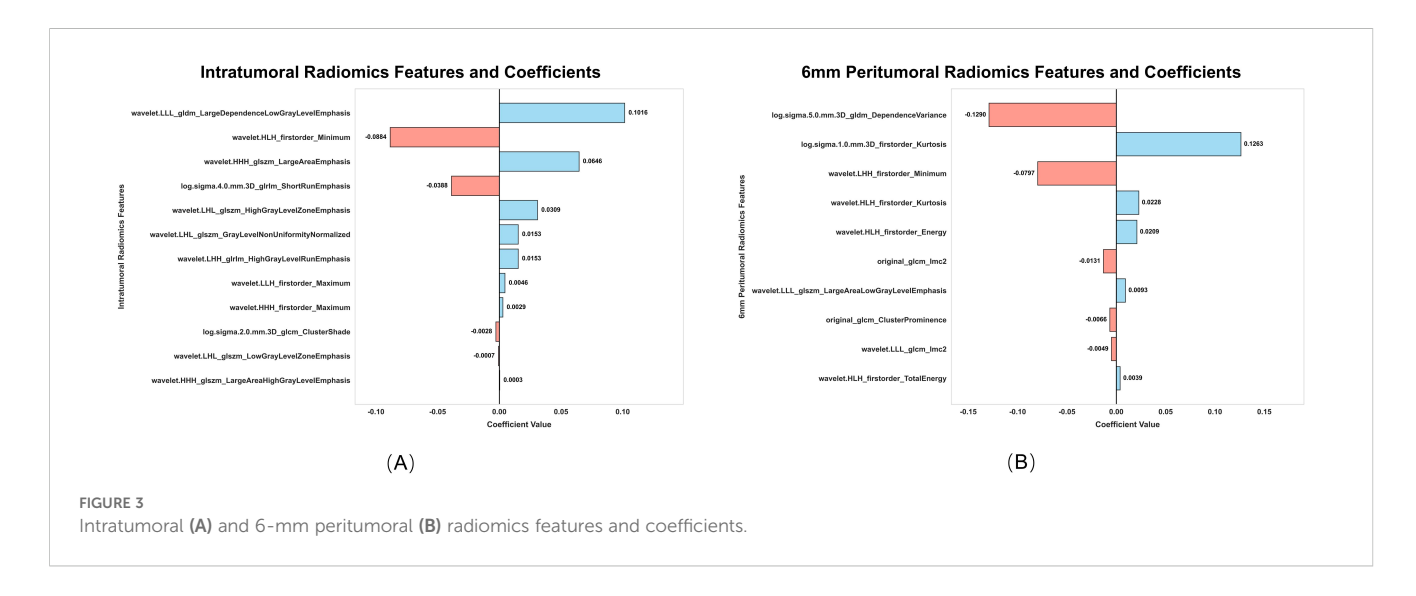
Rad: Intratumoral radiomics signature. Rad_3mm, Rad_6mm, Rad_9mm: Peritumoral radiomics signatures with 3 mm, 6 mm, and 9 mm expansion distances, respectively.

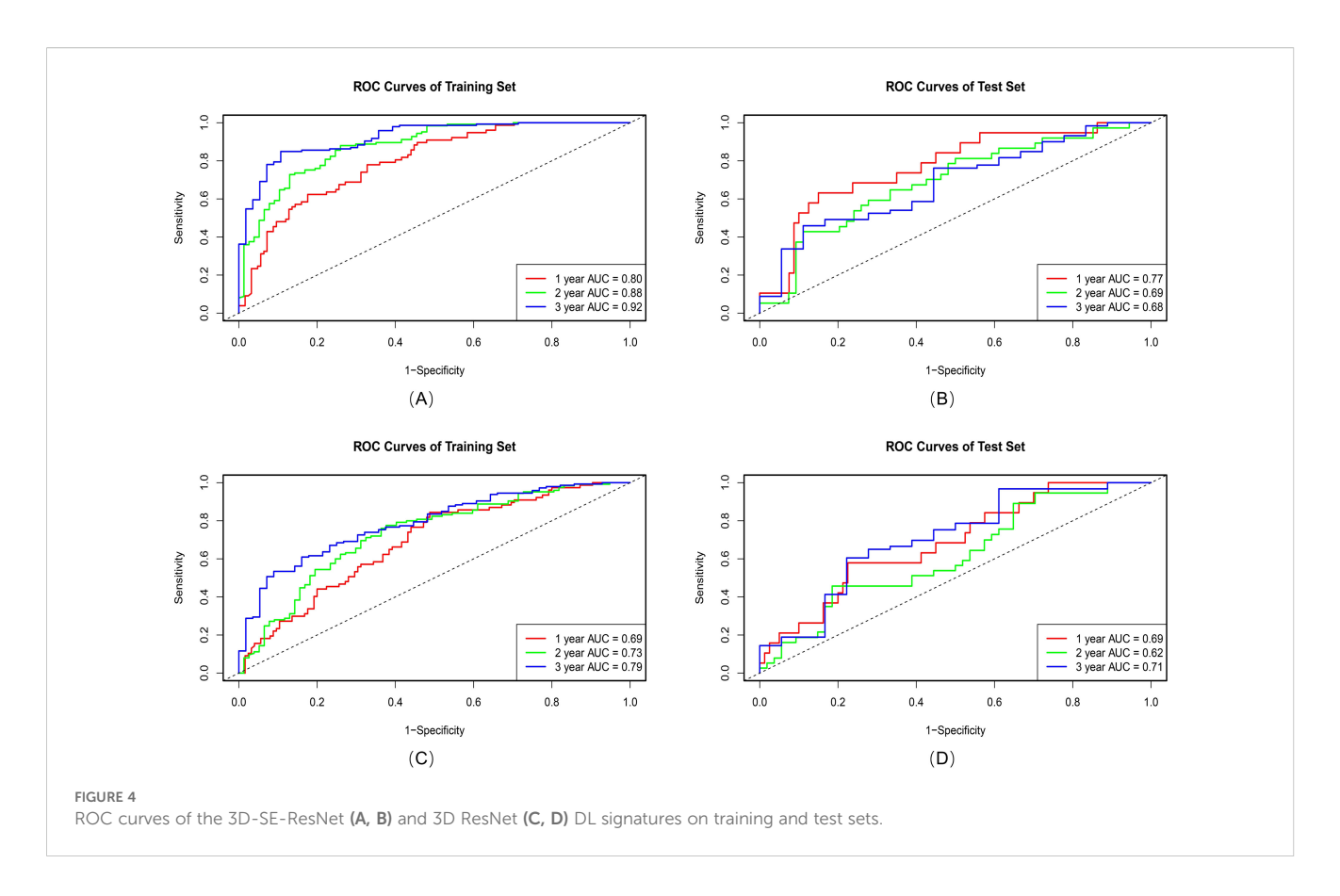
cancer at tumor margins (28). This complex tumor-host interface is often overlooked in traditional intratumoral radiomics (29). Liu et al. (30) demonstrated that peritumoral regions within 3–9 mm from the tumor boundary contain biological information relevant to lung cancer heterogeneity, suggesting that bidirectional tumor-host interactions at the interface critically influence prognosis. Through systematic evaluation of peritumoral regions at varying extents (3/6/9 mm), we identified the 6-mm peritumoral zone as optimal for balancing microenvironmental information capture and noise reduction (C-index=0.63), with further performance improvement when this zone was combined with intratumoral features (C-index=0.65). These findings indicate that peritumoral regions provide complementary information to intratumoral areas, supporting the hypothesis that peritumoral regions serve as pathways for tumor invasion (12, 15). Compared with single-

center studies (31), our multicenter validation confirms the generalizability of peritumoral radiomics, suggesting its clinical applicability.

3D CNNs enable precise spatial characterization of tumors through the integration of continuous cross-sectional information (32, 33). Wang et al. demonstrated the superior performance of 3D DL features over 2D methods in predicting occult lymph node metastasis in patients with laryngeal squamous cell carcinoma (AUC = 0.89 vs 0.86) (21). However, tumor heterogeneity leads to significant variations in prognostic contributions from different feature channels, and conventional CNNs lack the ability to prioritize critical features. To address this limitation, we innovatively integrated the SE module into the 3D ResNet framework. The SE module compresses spatial dimensions via global average pooling and learns channelwise weights through fully connected layers. This process achieves adaptive recalibration of feature maps, enhancing the expression of prognosis-relevant information while suppressing redundant signals (34). Ablation experiments demonstrated the critical role of the SE module: the 3D-SE-ResNet model exhibited a 13.8% improvement in the Cindex (0.74 vs. 0.65) compared to the baseline 3D-ResNet, highlighting its ability to resolve spatial heterogeneity through attention-driven feature calibration.

The hierarchical representation capability of deep neural networks enables 3D-SE-ResNet to capture complex tumor-host interface patterns that are challenging to quantify with traditional handcrafted features, corroborating prior studies highlighting deep learning's advantages in high-dimensional feature representation (35, 36). The combined model achieved increased predictive accuracy by synergistically integrating intratumoral/peritumoral radiomics information with DL-derived spatial hierarchical features, transcending the limitations of single-prediction modalities. PCA revealed multidimensional feature contributions: PC1 demonstrated balanced contributions from intratumoral/peritumoral radiomics features and deep learning features, indicating synergistic integration among the three feature classes. PC2 was dominated by DL features, reflecting the significant representational power of 3D CNNs in capturing macroscale





tumor spatial heterogeneity (37). The performance of the peritumoral radiomics features was greatest for PC3, which is consistent with the findings from the radiomics analysis in the optimal 6 mm peritumoral region. This synergy underscores the unique value of multidimensional integration in decoding tumor complexity.

In this study, the difference in median survival time between the training and test sets may be partially attributed to the gradual adoption of precise radiotherapy technologies such as image-guided radiotherapy during the multicenter data collection period. Although we controlled confounding factors through uniform inclusion criteria, the retrospective design inherently limits the elimination of selection bias. Notably, prolonged survival itself

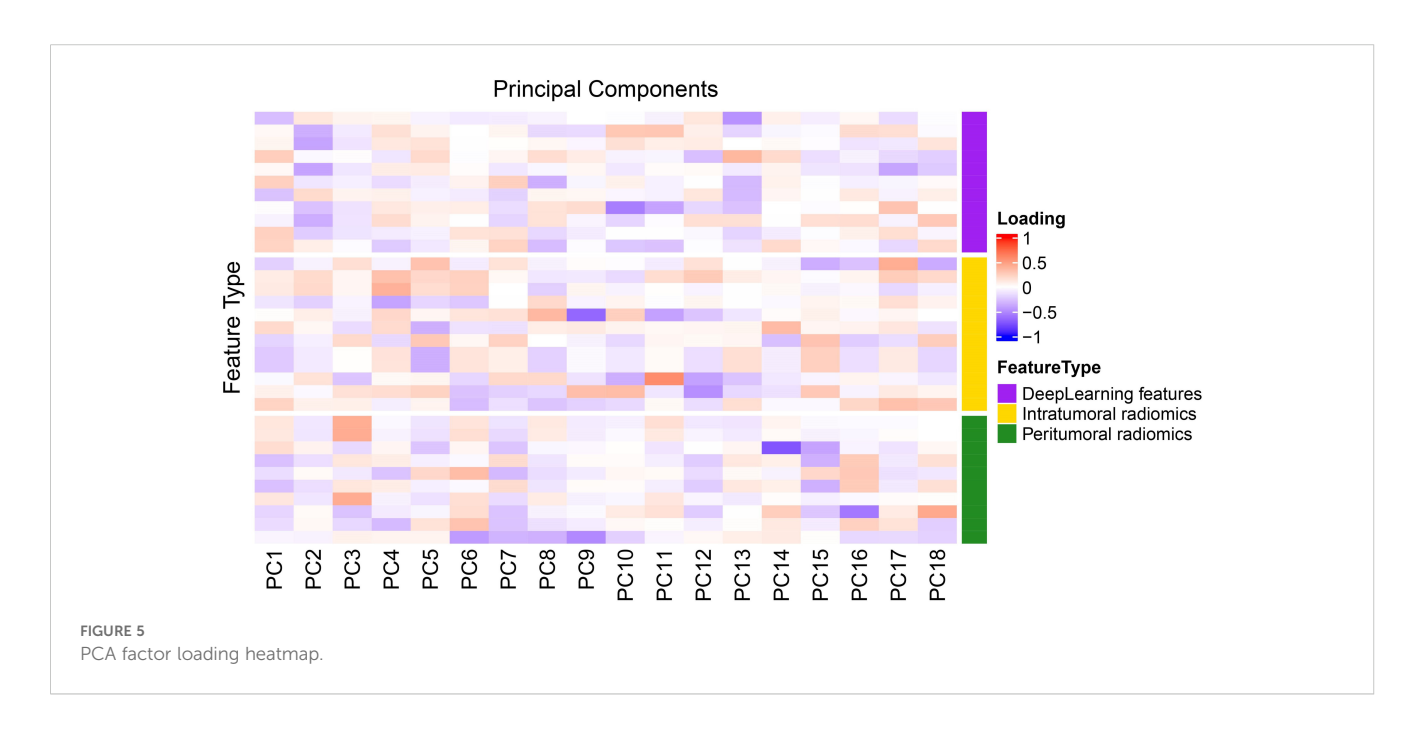


TABLE 4 AUC (95%CI) of intratumoral/peritumoral radiomics signatures, deep learning signatures, and combined model for 1-, 2-, and 3-year OS in patients.

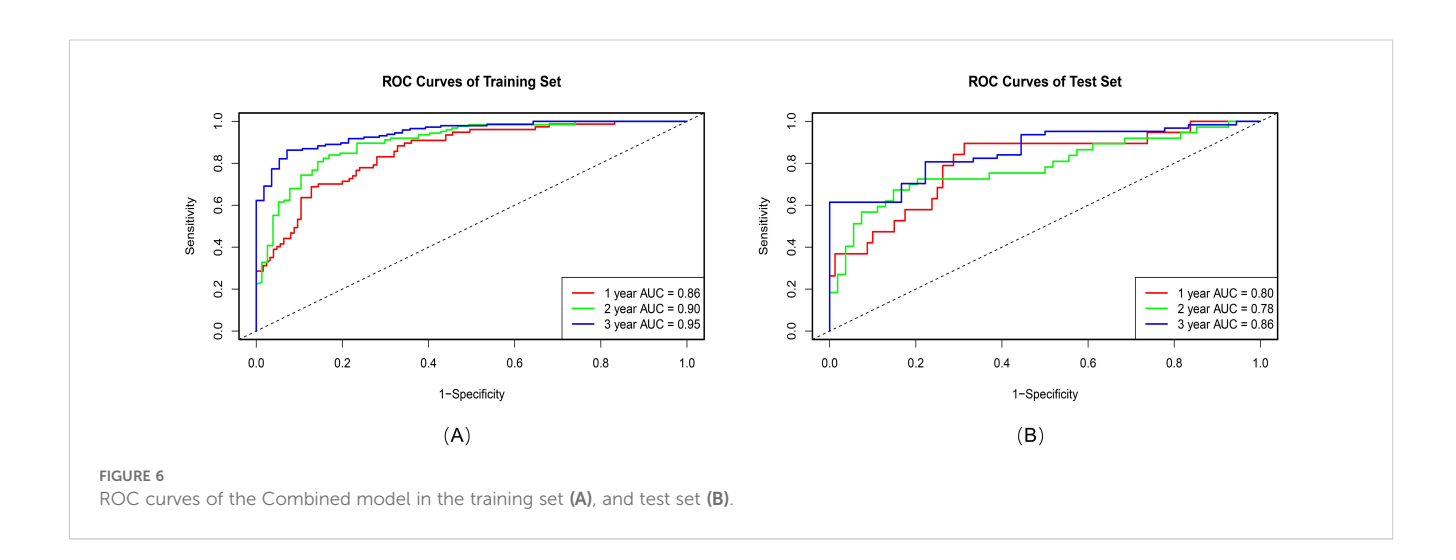
Models	AUC	Training set	Test set	P value
Rad	1-year	0.68 (0.61-0.75)	0.64 (0.50-0.78)	0.03
	2-year	0.69 (0.61-0.76)	0.64 (0.52-0.75)	0.02
	3-year	0.76 (0.68-0.83)	0.66 (0.50-0.81)	<0.01
Rad_6mm	1-year	0.70 (0.63-0.77)	0.64 (0.50-0.79)	0.01
	2-year	0.71 (0.63-0.77)	0.71 (0.60-0.82)	0.2
	3-year	0.71 (0.63-0.79)	0.67 (0.53-0.80)	0.02
DL	1-year	0.80 (0.74-0.85)	0.77 (0.66-0.88)	0.5
	2-year	0.88 (0.83-0.92)	0.69 (0.58-0.80)	0.05
	3-year	0.92 (0.88-0.96)	0.68 (0.55-0.82)	< 0.01
Combined Model	1-year	0.86 (0.81-0.90)	0.80 (0.69-0.91)	_
	2-year	0.90 (0.86-0.94)	0.78 (0.68-0.88)	_
	3-year	0.95 (0.92-0.97)	0.86 (0.77-0.94)	_

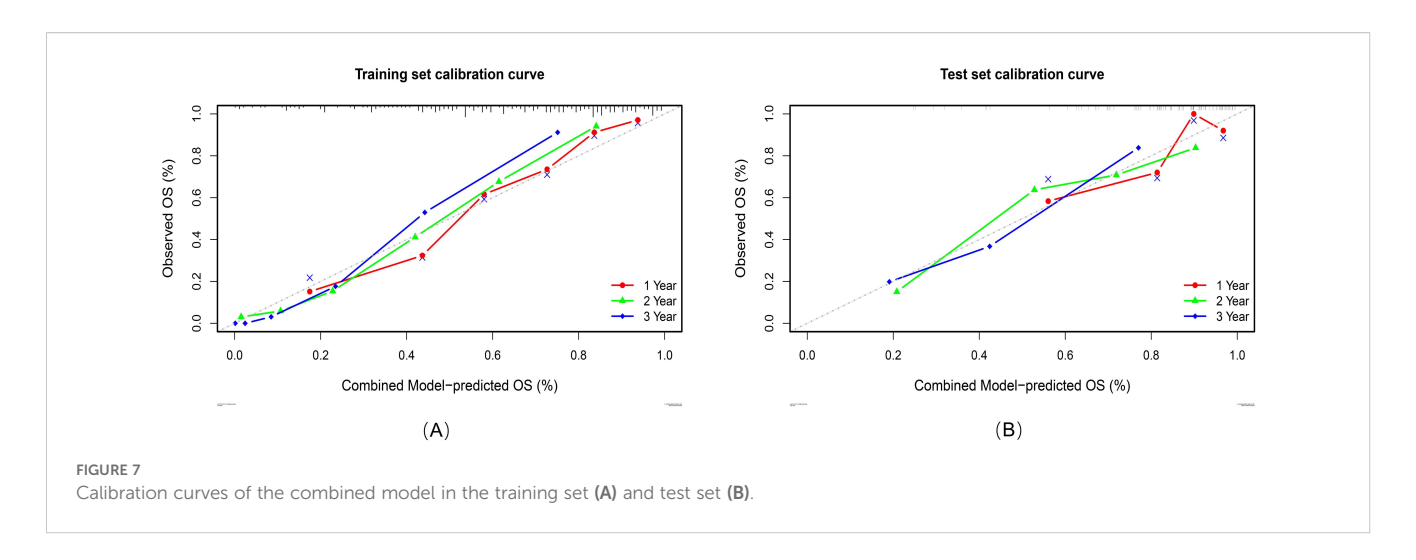
Boldface values indicate the best predictive performance.

The P values from the DeLong test compare individual signatures with the Combined Model in the test set.

may reflect therapeutic advancements rather than model prediction bias, providing unique insights into model robustness evaluation within evolving technological contexts. The drop in the combined model's C-index from the training set (0.77) to the test set (0.73) is a typical manifestation of model generalization across distinct datasets. The training and test sets originate from different medical centers, leading to inevitable discrepancies in patient

demographics, treatment details, and data distribution patterns. Despite this decline, the test set C-index of 0.73 still denotes satisfactory predictive performance. To enhance the generalization capability, three key countermeasures were implemented: (1) Integration of L2 regularization (λ =1e-4) with dropout layers (rate=0.4) in the DL framework to prevent overfitting to short-term survival signals; (2) PCA-based feature





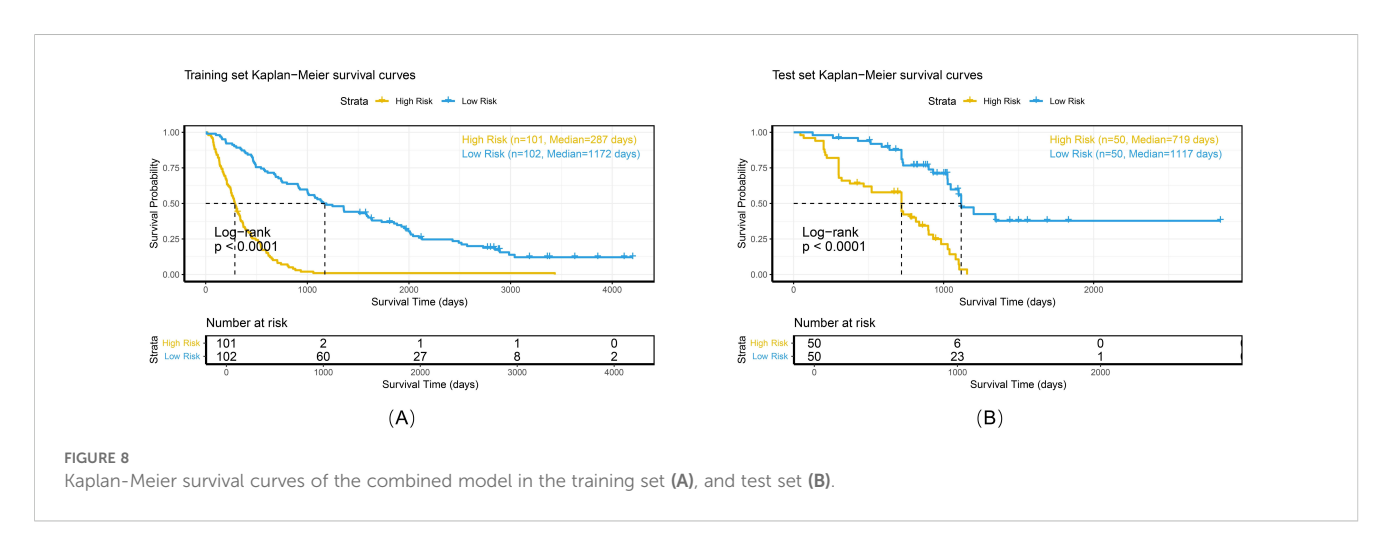
fusion preserving 95% variance to effectively mitigate multisource data noise; and (3) bootstrap calibration validation demonstrating strong consistency between the predicted probabilities and observed survival rates in the test set. Importantly, the model maintained stable discriminative performance (C-index=0.73) and significant risk stratification capacity (log-rank P < 0.001) in the test set, indicating its tolerance to moderate prognostic distribution shifts.

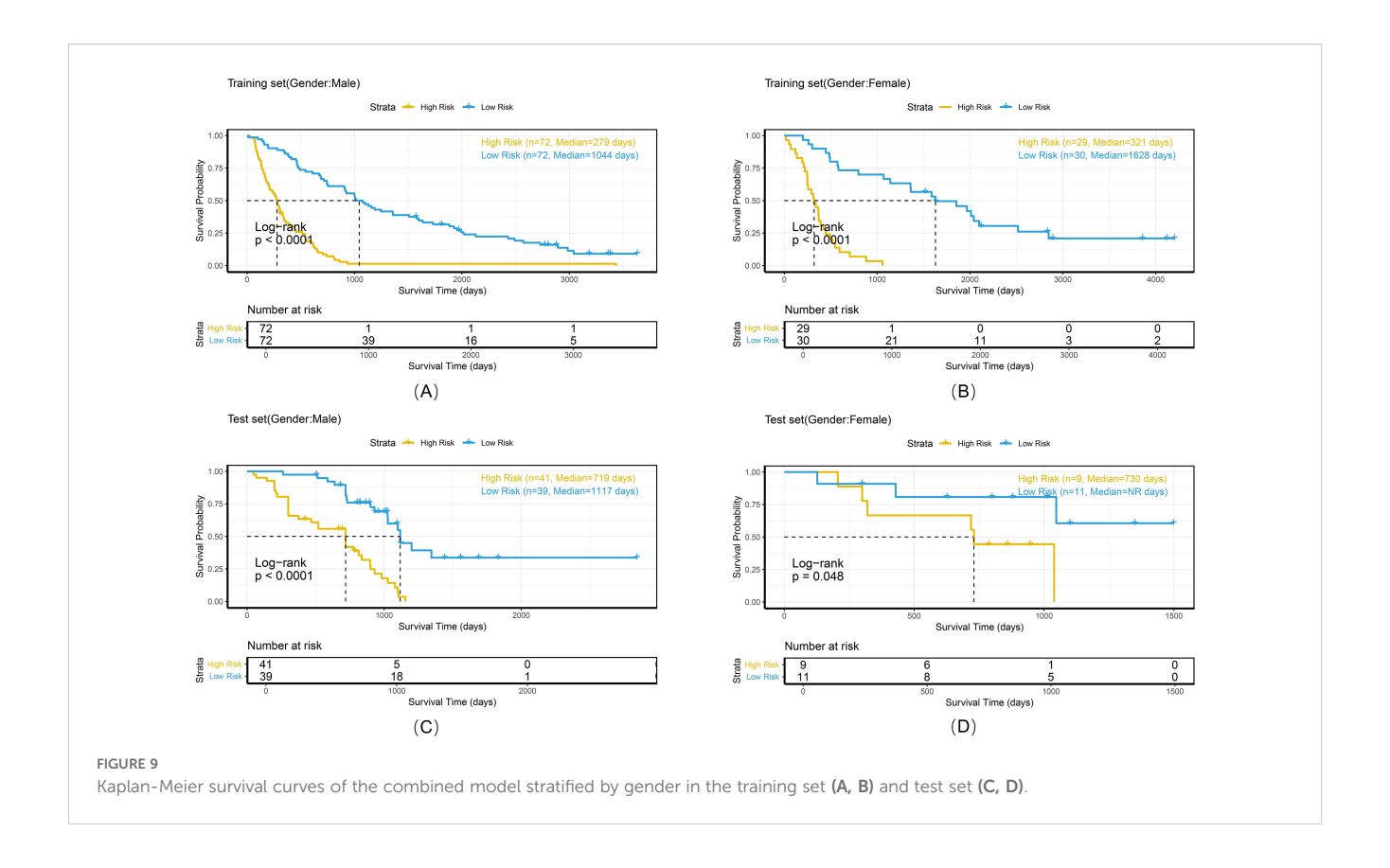
The combined model demonstrated stable risk stratification capabilities across multicenter datasets, enabling individualized prognostic assessments during RT planning for NSCLC patients. Subgroup analyses (by gender, age, histologic subtype, and overall stage) further validated the model's potential for personalized risk assessment. For example, in the <65 years and ≥65 years subgroups, both the training and test sets exhibited strong risk stratification capacity with consistent HR trends (training set: 7.28 vs. 3.88; test set: 3.37 vs. 5.94). Similarly, in adenocarcinoma and squamous cell carcinoma subgroups, the model maintained stable discriminative power (training set: 4.88 vs. 7.18; test set: 2.94 vs. 5.07), with statistically significant survival differences observed in all subgroups. These findings confirm that despite minor differences between cohorts, the model retains stable prognostic utility, supporting its potential for cross-population clinical application. Risk-based stratification identifies candidates who may benefit from high-dose irradiation, whereas quantitative analysis of peritumoral radiomics features aids in precisely delineating the boundaries of the clinical target volume (CTV).

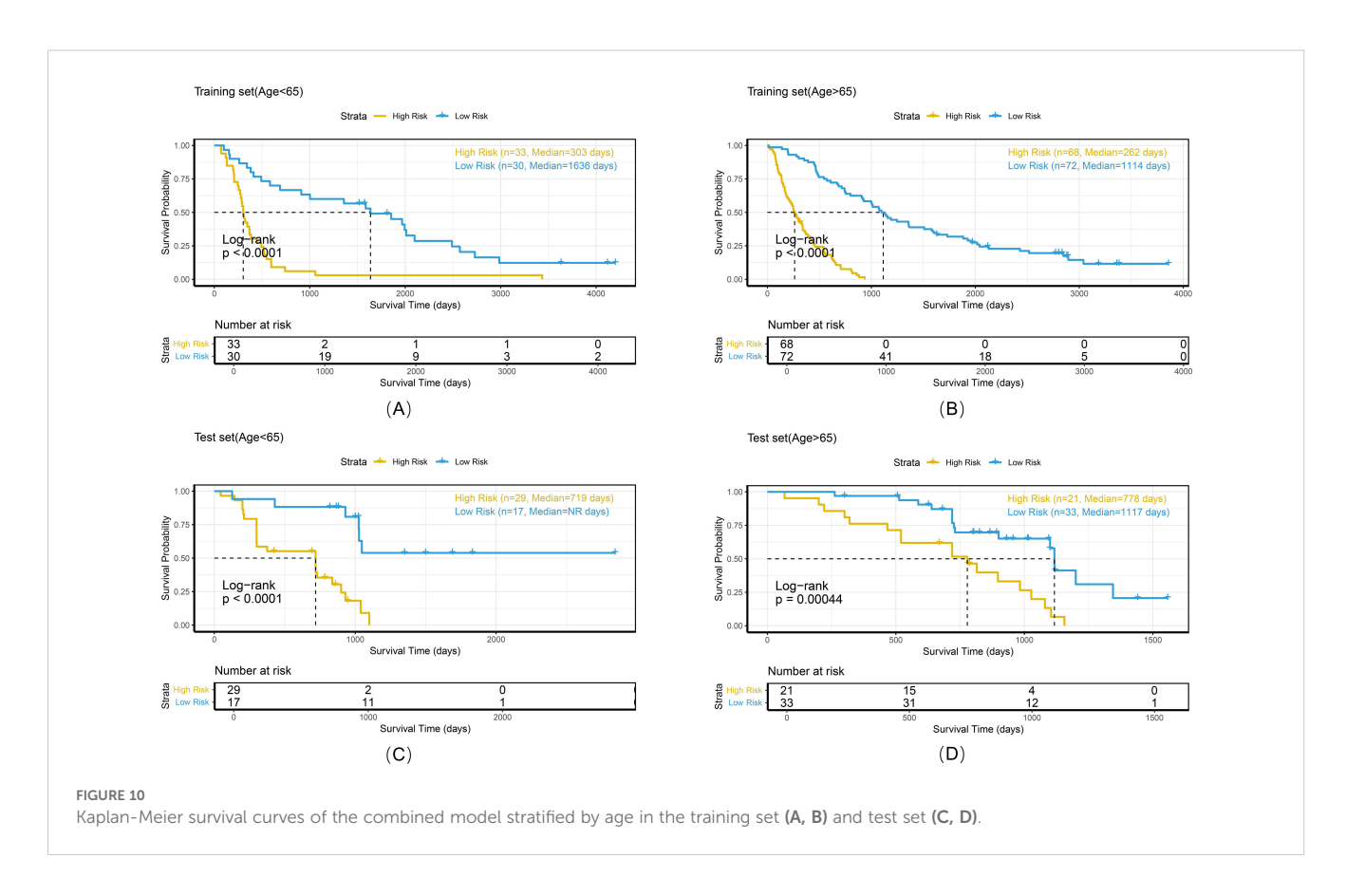
However, several limitations still exist: (1) retrospective design risks selection bias, necessitating prospective validation; (2) unclear biological basis of the 6-mm extension needs histopathological correlation; (3) due to the lack of detailed records on whether each patient received chemoradiotherapy or radiotherapy alone, we were unable to analyze the potential impact of these two treatment modalities on the study results. Future studies should integrate multi-omics data to unravel imaging–microenvironment molecular correlations, incorporate dosiomics to explore dose–response relationships, and collect detailed records of treatment modalities (e.g., radiotherapy alone vs. chemoradiotherapy) to clarify their impact on outcomes. Additionally, developing explainability tools to demystify model decisions will enhance clinical credibility.

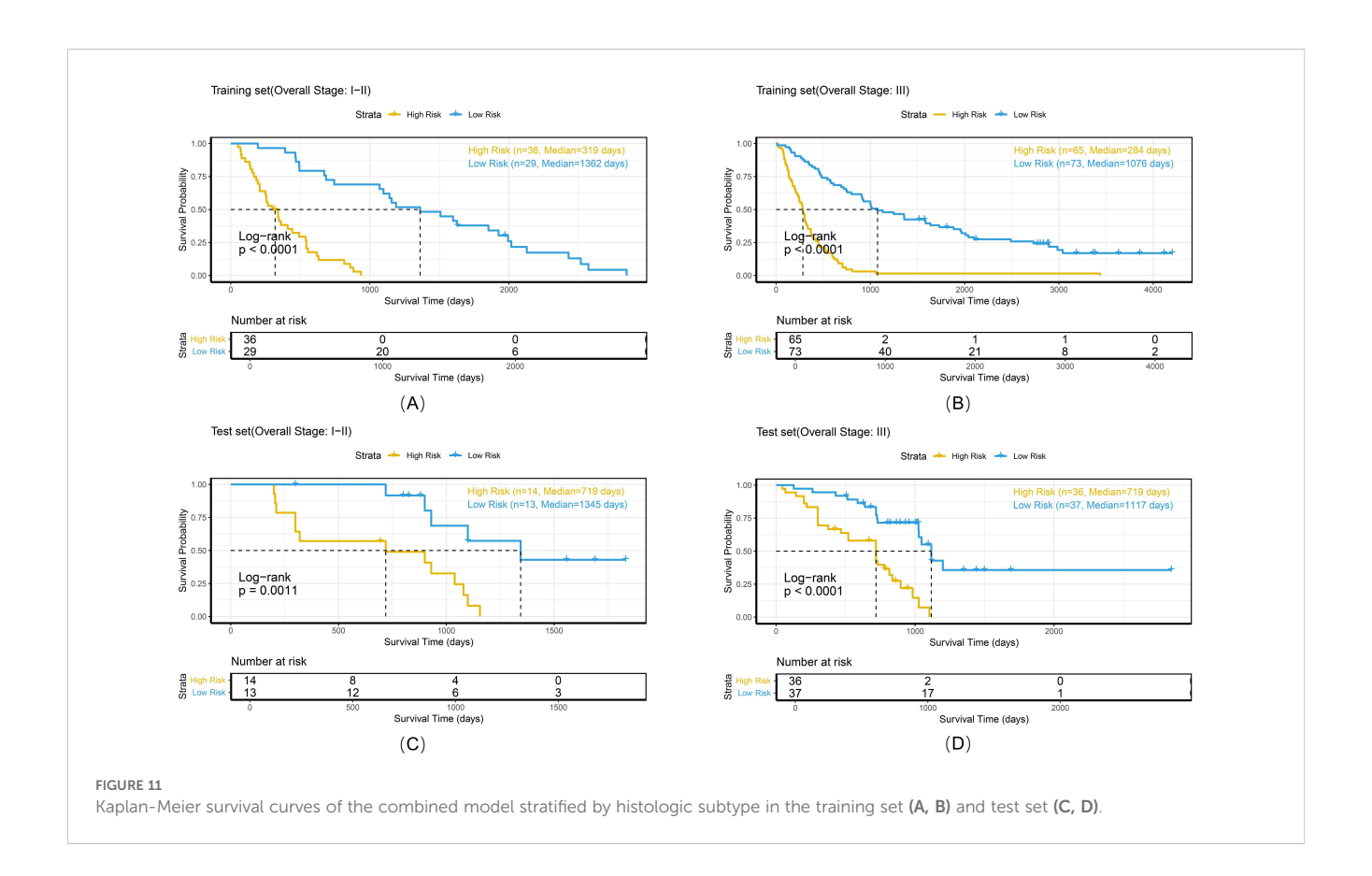
Conclusion

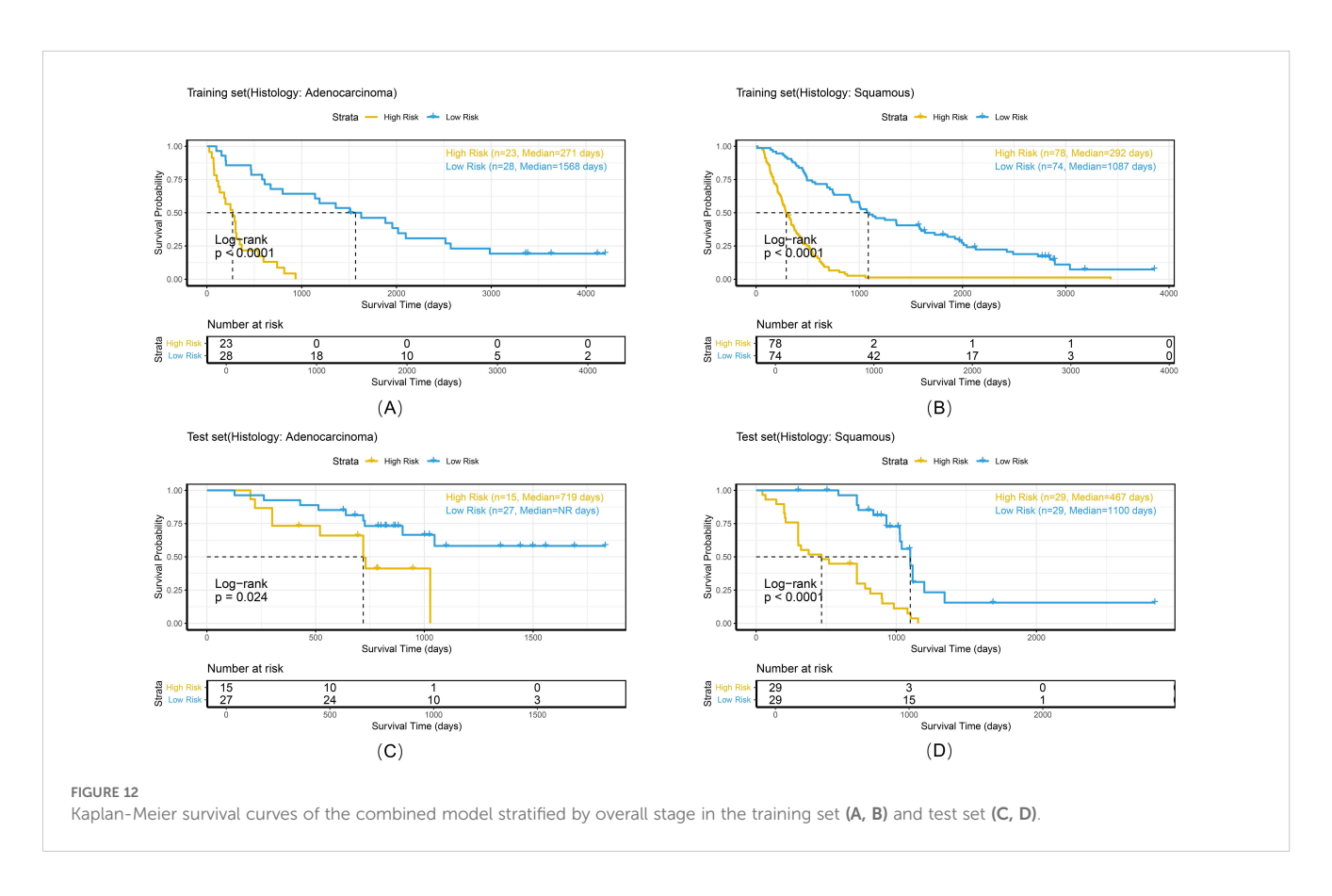
In conclusion, our multicenter-validated model, which integrates intratumoral, 6-mm peritumoral radiomics, and 3D DL features, significantly improves survival prediction in NSCLC











patients receiving radiotherapy. Future efforts will focus on prospective validation and mechanistic exploration of the model's biological foundations.

Data availability statement

The original contributions presented in the study are included in the article/supplementary material. Further inquiries can be directed to the corresponding authors.

Ethics statement

This study was approved by the Ethics Committees of the Seventh Medical Center of Chinese PLA General Hospital (No. S2025-030-01) and Shandong First Medical University (No. SB-KJCX2101). The studies were conducted in accordance with the local legislation and institutional requirements. Written informed consent for participation was not required from the participants or the participants' legal guardians/next of kin in accordance with the national legislation and institutional requirements.

Author contributions

YL: Conceptualization, Methodology, Software, Visualization, Writing – original draft. YP: Validation, Investigation, Writing – original draft. QW: Conceptualization, Methodology, Writing – review & editing. HJ: Investigation, Writing – review & editing. NL: Investigation, Writing – review & editing. DC: Investigation, Writing – review & editing. YY: Data Curation, Writing – original draft. YG: Data Curation, Writing – original draft. HZ: Data Curation, Writing – review & editing. YS: Investigation, Project administration, Resources, Writing – review & editing. JQ: Investigation, Project administration, Resources, Writing – review

& editing. FZ: Conceptualization, Investigation, Methodology, Project administration, Supervision, Validation, Funding acquisition, Writing – review & editing.

Funding

The author(s) declare that no financial support was received for the research and/or publication of this article.

Conflict of interest

The authors declare that the research was conducted in the absence of any commercial or financial relationships that could be construed as a potential conflict of interest.

Generative AI statement

The author(s) declare that no Generative AI was used in the creation of this manuscript.

Any alternative text (alt text) provided alongside figures in this article has been generated by Frontiers with the support of artificial intelligence and reasonable efforts have been made to ensure accuracy, including review by the authors wherever possible. If you identify any issues, please contact us.

Publisher's note

All claims expressed in this article are solely those of the authors and do not necessarily represent those of their affiliated organizations, or those of the publisher, the editors and the reviewers. Any product that may be evaluated in this article, or claim that may be made by its manufacturer, is not guaranteed or endorsed by the publisher.

References

- 1. Siegel RL, Miller KD, Fuchs HE, Jemal A. Cancer statistics, 2022. *CA Cancer J Clin.* (2022) 72:7–33. doi: 10.3322/caac.21708
- 2. Bray F, Laversanne M, Sung H, Ferlay J, Siegel RL, Soerjomataram I, et al. Global cancer statistics 2022: GLOBOCAN estimates of incidence and mortality worldwide for 36 cancers in 185 countries. *CA Cancer J Clin.* (2024) 74:229–63. doi: 10.3322/casc.21834
- 3. Chen P, Liu Y, Wen Y, Zhou C. Non-small cell lung cancer in China. Cancer Commun (Lond). (2022) 42:937–70. doi: 10.1002/cac2.12359
- 4. Vinod SK, Hau E. Radiotherapy treatment for lung cancer: Current status and future directions. Respirology. (2020) 25:61-71. doi: 10.1111/resp.13870
- 5. Bradley JD, Hu C, Komaki RR, Masters GA, Blumenschein GR, Schild SE, et al. Long-term results of NRG oncology RTOG 0617: standard- versus high-dose chemoradiotherapy with or without cetuximab for unresectable stage III non-small-cell lung cancer. *J Clin Oncol.* (2020) 38:706–14. doi: 10.1200/JCO.19.01162
- 6. Riely GJ, Wood DE, Ettinger DS, Aisner DL, Akerley W, Bauman JR, et al. Nonsmall cell lung cancer, version 4.2024, NCCN clinical practice guidelines in oncology. *J Natl Compr Canc Netw.* (2024) 22:249–74. doi: 10.6004/jnccn.2204.0023

- 7. Relli V, Trerotola M, Guerra E, Alberti S. Abandoning the notion of non-small cell lung cancer. *Trends Mol Med.* (2019) 25:585–94. doi: 10.1016/j.molmed.2019.04.012
- 8. Goldstraw P, Chansky K, Crowley J, Rami-Porta R, Asamura H, Eberhardt WEE, et al. The IASLC lung cancer staging project: proposals for revision of the TNM stage groupings in the forthcoming (Eighth) edition of the TNM classification for lung cancer. *J Thorac Oncol.* (2016) 11:39–51. doi: 10.1016/j.jtho.2015.09.009
- 9. Lambin P, Rios-Velazquez E, Leijenaar R, Carvalho S, Van Stiphout RGPM, Granton P, et al. Radiomics: extracting more information from medical images using advanced feature analysis. *Eur J Cancer*. (2012) 48:441–6. doi: 10.1016/j.ejca.2011.11.036
- 10. Zhao M, Kluge K, Papp L, Grahovac M, Yang S, Jiang C, et al. Multi-lesion radiomics of PET/CT for non-invasive survival stratification and histologic tumor risk profiling in patients with lung adenocarcinoma. *Eur Radiol.* (2022) 32:7056–67. doi: 10.1007/s00330-022-08999-7
- 11. Zhang X, Lu B, Yang X, Lan D, Lin S, Zhou Z, et al. Prognostic analysis and risk stratification of lung adenocarcinoma undergoing EGFR-TKI therapy with time-serial

CT-based radiomics signature. $\it Eur~Radiol.~(2023)~33:825-35.~doi:~10.1007/s00330-022-09123-5$

- 12. Kadota K, Nitadori J-I, Sima CS, Ujiie H, Rizk NP, Jones DR, et al. Tumor Spread through Air Spaces is an Important Pattern of Invasion and Impacts the Frequency and Location of Recurrences after Limited Resection for Small Stage I Lung Adenocarcinomas. *J Thorac Oncol.* (2015) 10:806–14. doi: 10.1097/
- 13. Onozato ML, Kovach AE, Yeap BY, Morales-Oyarvide V, Klepeis VE, Tammireddy S, et al. Tumor islands in resected early-stage lung adenocarcinomas are associated with unique clinicopathologic and molecular characteristics and worse prognosis. *Am J Surg Pathol.* (2013) 37:287–94. doi: 10.1097/PAS.0b013e31826885fb
- 14. Uruga H, Fujii T, Fujimori S, Kohno T, Kishi K. Semiquantitative assessment of tumor spread through air spaces (STAS) in early-stage lung adenocarcinomas. *J Thorac Oncol.* (2017) 12:1046–51. doi: 10.1016/j.jtho.2017.03.019
- 15. Khorrami M, Khunger M, Zagouras A, Patil P, Thawani R, Bera K, et al. Combination of peri- and intratumoral radiomic features on baseline CT scans predicts response to chemotherapy in lung adenocarcinoma. *Radiol Artif Intell.* (2019) 1: e180012. doi: 10.1148/ryai.2019180012
- 16. Chen Q, Shao J, Xue T, Peng H, Li M, Duan S, et al. Intratumoral and peritumoral radiomics nomograms for the preoperative prediction of lymphovascular invasion and overall survival in non-small cell lung cancer. *Eur Radiol.* (2023) 33:947–58. doi: 10.1007/s00330-022-09109-3
- $17.\,$ Wu L, Lou X, Kong N, Xu M, Gao C. Can quantitative peritumoral CT radiomics features predict the prognosis of patients with non-small cell lung cancer? A systematic review. Eur Radiol. (2023) 33:2105–17. doi: 10.1007/s00330-022-09174-8
- 18. Lin P, Xie W, Li Y, Zhang C, Wu H, Wan H, et al. Intratumoral and peritumoral radiomics of MRIs predicts pathologic complete response to neoadjuvant chemoimmunotherapy in patients with head and neck squamous cell carcinoma. *J Immunother Cancer*. (2024) 12:e009616. doi: 10.1136/jitc-2024-009616
- Xiao ML, Fu L, Wei Y, Liu AE, Cheng JJ, Ma FH, et al. Intratumoral and peritumoral MRI radiomics nomogram for predicting parametrial invasion in patients with early-stage cervical adenocarcinoma and adenosquamous carcinoma. Eur Radiol. (2024) 34:852–62. doi: 10.1007/s00330-023-10042-2
- 20. Bao X, Peng Q, Bian D, Ni J, Zhou S, Zhang P, et al. Short-term intra- and peritumoral spatiotemporal CT radiomics for predicting major pathological response to neoadjuvant chemoimmunotherapy in non-small cell lung cancer. *Eur Radiol.* (2025), 35:1–13. doi: 10.1007/s00330-025-11563-8
- 21. Wang W, Liang H, Zhang Z, Xu C, Wei D, Li W, et al. Comparing three-dimensional and two-dimensional deep-learning, radiomics, and fusion models for predicting occult lymph node metastasis in laryngeal squamous cell carcinoma based on CT imaging: a multicentre, retrospective, diagnostic study. *EClinicalMedicine*. (2024) 67:102385. doi: 10.1016/j.eclinm.2023.102385
- 22. Nie D, Lu J, Zhang H, Adeli E, Wang J, Yu Z, et al. Multi-channel 3D deep feature learning for survival time prediction of brain tumor patients using multi-modal neuroimages. *Sci Rep.* (2019) 9:1103. doi: 10.1038/s41598-018-37387-9
- 23. Shen T, Hou R, Ye X, Li X, Xiong J, Zhang Q, et al. Predicting Malignancy and invasiveness of pulmonary subsolid nodules on CT images using deep learning. *Front Oncol.* (2021) 11:700158. doi: 10.3389/fonc.2021.700158
- 24. Aerts HJWL, Wee L, Rios Velazquez E, Leijenaar RTH, Parmar C, Grossmann P, et al. Data from NSCLC-radiomics. *Nat Commun* (2019) 5:4006. doi: 10.7937/K9/TCIA.2015.PF0M9REI

- 25. Katzman JL, Shaham U, Cloninger A, Bates J, Jiang T, Kluger Y. DeepSurv: personalized treatment recommender system using a Cox proportional hazards deep neural network. *BMC Med Res Methodol.* (2018) 18:24. doi: 10.1186/s12874-018-0482-1
- 26. Hindocha S, Charlton TG, Linton-Reid K, Hunter B, Chan C, Ahmed M, et al. A comparison of machine learning methods for predicting recurrence and death after curative-intent radiotherapy for non-small cell lung cancer: Development and validation of multivariable clinical prediction models. *EBioMedicine*. (2022) 77:103911. doi: 10.1016/j.ebiom.2022.103911
- 27. Zhang L, Xu C, Zhang X, Wang J, Jiang H, Chen J, et al. A novel analytical approach for outcome prediction in newly diagnosed NSCLC based on [18F]FDG PET/CT metabolic parameters, inflammatory markers, and clinical variables. *Eur Radiol.* (2023) 33:1757–68. doi: 10.1007/s00330-022-09150-2
- 28. Saijo T, Ishii G, Ochiai A, Hasebe T, Yoshida J, Nishimura M, et al. Evaluation of extratumoral lymphatic permeation in non-small cell lung cancer as a means of predicting outcome. *Lung Cancer*. (2007) 55:61–6. doi: 10.1016/j.lungcan.2006.09.027
- 29. Pérez-Morales J, Tunali I, Stringfield O, Eschrich SA, Balagurunathan Y, Gillies RJ, et al. Peritumoral and intratumoral radiomic features predict survival outcomes among patients diagnosed in lung cancer screening. *Sci Rep.* (2020) 10:10528. doi: 10.1038/s41598-020-67378-8
- 30. Liu K, Li K, Wu T, Liang M, Zhong Y, Yu X, et al. Improving the accuracy of prognosis for clinical stage I solid lung adenocarcinoma by radiomics models covering tumor per se and peritumoral changes on CT. *Eur Radiol.* (2022) 32:1065–77. doi: 10.1007/s00330-021-08194-0
- 31. Chang R, Qi S, Wu Y, Yue Y, Zhang X, Qian W. Nomograms integrating CT radiomic and deep learning signatures to predict overall survival and progression-free survival in NSCLC patients treated with chemotherapy. *Cancer Imaging*. (2023) 23:101. doi: 10.1186/s40644-023-00620-4
- 32. Bathla G, Dhruba DD, Liu Y, Le NH, Soni N, Zhang H, et al. Differentiation between glioblastoma and metastatic disease on conventional MRI imaging using 3D-convolutional neural networks: model development and validation. *Acad Radiol.* (2024) 31:2041–9. doi: 10.1016/j.acra.2023.10.044
- 33. Zhao X, Zhou B, Luo Y, Chen L, Zhu L, Chang S, et al. CT-based deep learning model for predicting hospital discharge outcome in spontaneous intracerebral hemorrhage. *Eur Radiol.* (2024) 34:4417–26. doi: 10.1007/s00330-023-10505-6
- 34. Hu J, Shen L, Albanie S, Sun G, Wu E. Squeeze-and-excitation networks. *IEEE Trans Pattern Anal Mach Intell.* (2020) 42:2011–23. doi: 10.1109/TPAMI.2019.2913372
- 35. Schön F, Kieslich A, Nebelung H, Riediger C, Hoffmann R-T, Zwanenburg A, et al. Comparative analysis of radiomics and deep-learning algorithms for survival prediction in hepatocellular carcinoma. *Sci Rep.* (2024) 14:590. doi: 10.1038/s41598-023-50451-3
- 36. Liu Y, Wang Y, Hu X, Wang X, Xue I, Pang Q, et al. Multimodality deep learning radiomics predicts pathological response after neoadjuvant chemoradiotherapy for esophageal squamous cell carcinoma. *Insights Imaging*. (2024) 15:277. doi: 10.1186/s13244-024-01851-0
- 37. Huang B, Sollee J, Luo Y-H, Reddy A, Zhong Z, Wu J, et al. Prediction of lung Malignancy progression and survival with machine learning based on pretreatment FDG-PET/CT. *EBioMedicine*. (2022) 82:104127. doi: 10.1016/j.ebiom.2022.104127